DALTON
FULL PAPER

Organometallic platinum(II) complexes of methyl-substituted phenanthrolines †

Axel Klein,*[a] Eric J. L. McInnes[b] and Wolfgang Kaim[a]

[a] *Institut für Anorganische Chemie, Universität Stuttgart, Pfaffenwaldring 55, D-70550 Stuttgart, Germany*
[b] *EPSRC c.w. EPR Service Centre, Department of Chemistry, The University of Manchester, Manchester, UK M13 9PL*

Received 7th February 2002, Accepted 27th March 2002
First published as an Advance Article on the web 30th April 2002

A series of dimesitylplatinum(II) complexes of symmetrically substituted dimethyl-1,10-phenanthrolines (dmphen) was prepared and examined in view of their electronic structure. Electrochemical data of the parent complexes and spectroscopic data of parent and one-electron reduced species reveal the variable electronic influence of the methyl substituents in different positions of the heteroaromatic system. From multi-frequency S, X, K and Q-band EPR measurements of the corresponding radical anions and of analogous species with 1,10-phenanthroline, 3,4,7,8-tetramethyl-1,10-phenanthroline and 2,2′-bipyridine ligands hyperfine coupling constants and *g* values were obtained and used for an estimation of the contributions from platinum orbitals to the singly occupied molecular orbital. X-Ray crystal structures are reported for [(2,9-dmphen)$PtMes_2$] and [(2,9-dmphen)$PtPh_2$], allowing us to probe the steric interactions between the methyl substituents of the phenanthroline and the mesityl ligands.

Introduction

Organometallic complexes of 1,10-phenanthrolines and related α-diimine ligands with d^8 configurated M(II) centres (M = Ni, Pd, Pt) have gained enormous interest in the last few years due to their interesting photophysical and other optical properties[1–3] and their relevance in catalysis, especially in the oxidation of alkanes[4] or olefin polymerisation.[5] For 1,10-phenanthrolines, the rigid backbone and the accessibility of various substituted derivatives[6] is essential for systematic studies of the sterical and electronic effects of substituents.[7–9] In a previous contribution we have reported that 1,10-phenanthroline ligands exhibit different orbital occupation for one added electron, depending on the substitution pattern. In contrast to the anion radicals of 1,10-phenanthroline (phen)[8,10] and its 2,9-, 4,7- or 5,6-dimethyl derivatives (2,9-dmphen, 4,7-dmphen, 5,6-dmphen) with their $^2B_1$ ground state,[8] the 3,4,7,8-tetramethyl derivative $tmphen^{\bullet-}$ has a $^2A_2$ ground state (see Scheme 1 + 2).[7]

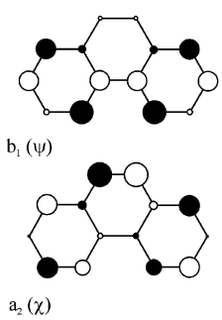

Scheme 1 Graphic representations of the $^2B_1$ (ψ) and $^2A_2$ (χ) LUMOs of 1,10-phenanthrolines from HMO type calculations, the balls represent relative electron density.

† Electronic supplementary information (ESI) available: Table S1 with data from ^{1}H-NMR spectroscopy and elemental analysis, Figs. S1 and S2 with representations of the crystal structures of [(2,9-dmphen)$PtMes_2$] and [(2,9-dmphen)Ph_2]. See http://www.rsc.org/suppdata/dt/b2/b201419j/

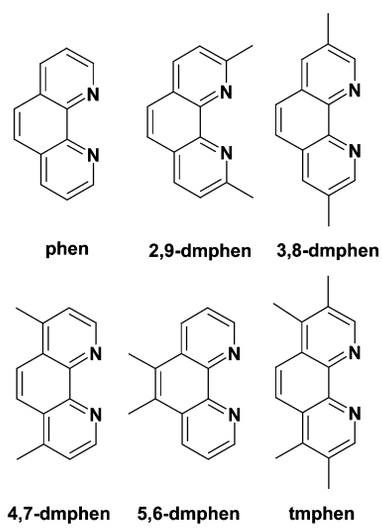

Scheme 2 The α-diimine ligand systems.

On coordination of transition metal atoms to the nitrogen donor atoms in a 1,10-position the $^2B_1$ situation should be favoured due to the higher relative electron density on the coordinating nitrogen atoms. In view of the generally weak bonding of platinum to these ligands, organometallic platinum(II) fragments seemed to be an interesting probe to establish whether the $^2A_2$ state is involved for 3,8-dmphen or tmphen.

For comparison, the 5,6-, 4,7- and 2,9-dimethyl derivatives and their new platinum(II) complexes were studied. The dimesitylplatinum fragment was chosen due to the high stability of the parent compounds and their ability to stabilise not only radical anion species with such ligands but also the monooxidized (cationic) states $[(NN)PtMes_2]^{\bullet+}$ of these complexes.[11,12] In regard of numerous reports on the special properties of the sterically demanding 2,9-dimethyl-1,10-phenanthroline (2,9-dmphen, neocuproine)[13–15] it was also of interest to examine more closely the corresponding complex [(2,9-dmphen)$PtMes_2$].

This journal is © The Royal Society of Chemistry 2002

Table 1 Crystallographic and structure refinement data

Compound	[(2,9-dmphen)$PtPh_2$]	[(2,9-dmphen)$PtMes_2$]
Empirical formula (M)	$C_{26}H_{22}N_2Pt$ (557.55)	$C_{32}H_{34}N_2Pt$ (641.70)
T/K	173(2)	183(2)
Crystal system, space group	Monoclinic, $P2_1/n$	Monoclinic, $P2_1/n$
a/Å	10.9215(11)	7.9365(11)
b/Å	15.7735(14)	21.999(3)
c/Å	11.8566(13)	15.287(3)
β/°	98.499(8)	93.662(14)
V/Å^3, Z	2020.1(4), 4	2663.6(7), 4
Calc. density/mg m^{-3}	1.833	1.600
μ/mm^{-1}, F(000)	6.96, 1080	5.29, 1272
θ-range/°	2.16 to 30.00	1.62 to 28.96
Limiting indices	$-1 \le h \le 15$, $-1 \le k \le 22$, $-16 \le l \le 16$	$-1 \le h \le 10$, $-1 \le k \le 29$, $-20 \le l \le 20$
Refl. collected., (independent)	7180, (5887)	8259, (6522)
R_{int}	0.0368	0.0639
Data/Restr./Param.	5887/0/285	6515/0/324
Goodness-of-fit on F^2 [a]	1.034	1.089
Final R indices [$I > 2\sigma(I)$] [b]	$R1 = 0.0345$, $wR2 = 0.0812$	$R1 = 0.0608$, $wR2 = 0.1203$
R indices (all data)	$R1 = 0.0493$, $wR2 = 0.0873$	$R1 = 0.1141$, $wR2 = 0.1629$
Δ_{max} peak and hole/e Å^{-3}	1.785 and −2.334	1.529 and −2.945

[a] GOF = $\{\Sigma w(|F_o|^2 - |F_c|^2)^2/(n - m)\}^{1/2}$; n = no. of reflections; m = no. of parameters. [b] $R = (||F_o| - |F_c||)/\Sigma F_o|$, $wR = \{\Sigma[w(|F_o|^2 - |F_c|^2)^2]/\Sigma[w(F_o^4)]\}^{1/2}$.

To understand the steric interference in this doubly hindered system the diphenylplatinum complex [(2,9-dmphen)$PtPh_2$] and the dimethylplatinum analogue [(2,9-dmphen)$PtMe_2$] were also prepared and examined.

The monoreduced complexes were investigated using EPR and UV/Vis/NIR spectroelectrochemical techniques. For EPR the multi-frequency approach [16] was essential to collect reliable data for the hyperfine coupling constants and g values.[17]

Results and discussion

Synthesis and general properties

The new complexes were synthesised in high yields according to established procedures (see Experimental section) and were correctly analyzed using ^{1}H-NMR spectroscopy and elemental analysis (see supplementary Table S1, see ESI †). In the ^{1}H-NMR spectra the occurrence of coupling to ^{195}Pt (I = 1/2, 33.8% nat. abundance) enabled us to unequivocally assign the protons. For the [(2,9-dmphen)$PtMes_2$] complex the signals for the hydrogen atoms located on the mesityl substituent show a slight deviation from the values found for the other complexes, probably due to an interaction of the mesityl substituents with the methyl groups on the phenanthroline (*vide infra*).

Crystal structure analysis of [(2,9-dmphen)$PtPh_2$] and [(2,9-dmphen)$PtMes_2$]

Suitable crystals were obtained by slow evaporation of toluene solutions and submitted to X-ray diffraction as described in the Experimental section and given in Table 1. There are no special intermolecular interactions other than van der Waals contacts, particularly no Pt ··· Pt contacts. This result is not unexpected for arylplatinum complexes,[7,11,17–20] it might also be anticipated from the steric properties of the 2,9-dmphen ligand. The molecular structures of the two complexes are shown in Fig. 1 and 2. To reveal the effects of interference between the mesityl substituents with the methyl groups on the phenanthroline ligand we compare the distances and angles found for the two molecules with those for the complex [(phen)$PtMes_2$] [7] in Tables 2 and 3. In Table 4 calculated structural data for the complexes are presented and compared with those of other platinum complexes of 2,9-dmphen.[13,14]

Evaluation of the data shows that the methyl substituents at the 2,9-position cause some structural deviation for the new complexes as compared to [(phen)$PtMes_2$]. C(1) and N(2) have longer distances to platinum than C(10) and N(1). This effect is most pronounced for the dimesityl complex. The average Pt–N bond lengths and the deviations from a best coordination plane [C(1)N(1)N(2)C(10)] are increased for the 2,9-dmphen complexes. The N(1)–Pt–N(2) angles, in contrast, do not change much. The 2,9-substitution thus has three main effects. First, the plane at the platinum(II) centre undergoes a tetrahedral distortion that is best illustrated by the dihedral angle ω for the two best planes [C(1)PtC(10)]–[N(1)C(39)C(29)N(2)]. The value of ω that is 31 or 42°, respectively, for the 2,9-dmphen complexes of $PtPh_2$ and $PtMes_2$ but only 6.4° for [(phen)Pt-Mes_2]. Secondly, the phenanthroline π planes twist relative away from the coordination planes. This can be seen by the dihedral angles for the best planes [N(1)PtN(2)] *vs.* [N(1)C(30)C(29)-N(2)] which are 23 or 28°, respectively, for the 2,9-dmphen complexes of $PtPh_2$ $PtMes_2$ but only 3.8° for the [(phen)$PtMes_2$]. The third effect is a marked loss of planarity of the phen ligand itself as revealed by the increased dihedral angles between the pyridyl moieties. Here the additional steric effect of the mesityl co-ligand compared to the phenyl group is very pronounced. It is also interesting to note that the two phenyl rings in [(2,9-dmphen)$PtPh_2$] do not orientate perpendicular to the square plane [19] but are tilted in nearly the same manner as the mesityl

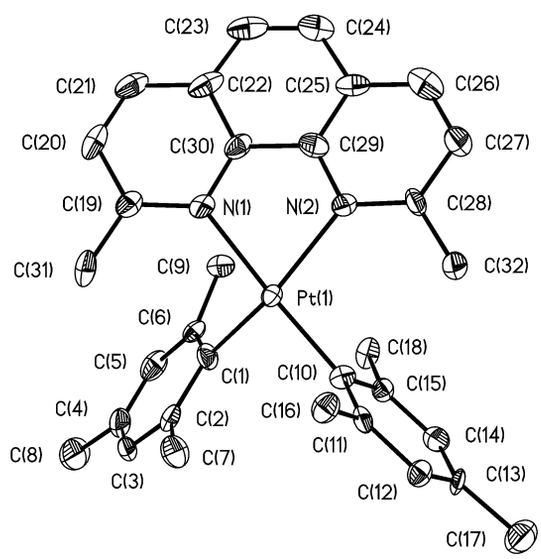

Fig. 1 Molecular structure of [(2,9-dmphen)$PtMes_2$].

Table 2 Bond lengths (Å) for [(2,9-dmphen)$PtPh_2$] and [(2,9-dmphen)$PtMes_2$] in comparison with [(phen)$PtMes_2$] (ref. 7)

	[(2,9-dmphen)$PtPh_2$]	[(2,9-dmphen)$PtMes_2$]	[(phen)$PtMes_2$]
Pt(1)–C(1)	2.007 (5)	2.027(9)	2.017(5)
Pt(1)–C10	1.993(5)	2.014(9)	2.015(5)
Pt(1)–N(1)	2.158(4)	2.117(8)	2.103(4)
Pt(1)–(N2)	2.147(4)	2.193(8)	2.108(4)
N(1)–C(19)	1.345(6)	1.364(13)	1.338(7)
N(1)–C(30)	1.374(6)	1.353(14)	1.372(7)
C(19)–C(20)	1.419(7)	1.423(14)	1.386(8)
C(20)–C(21)	1.370(8)	1.35(2)	1.362(9)
C(21)–C(22)	1.394(7)	1.42(2)	1.413(8)
C(22)–C(23)	1.425(7)	1.42(2)	1.431(9)
C(22)–C(30)	1.413(6)	1.433(14)	1.404(7)
C(23)–C(24)	1.365(8)	1.33(2)	1.346(8)
C(24)–C(25)	1.426(7)	1.45(2)	1.425(7)
C(25)–C(26)	1.399(7)	1.38(2)	1.401(8)
C(25)–C(29)	1.409(6)	1.41(2)	1.420(7)
C(26)–C(27)	1.361(8)	1.39(2)	1.380(8)
C(27)–C(28)	1.407(7)	1.410(14)	1.394(8)
C(28)–N(2)	1.340(6)	1.338(12)	1.327(7)
C(29)–N(2)	1.372(6)	1.370(13)	1.362(6)
C(29)–C(30)	1.432(6)	1.44(2)	1.428(7)

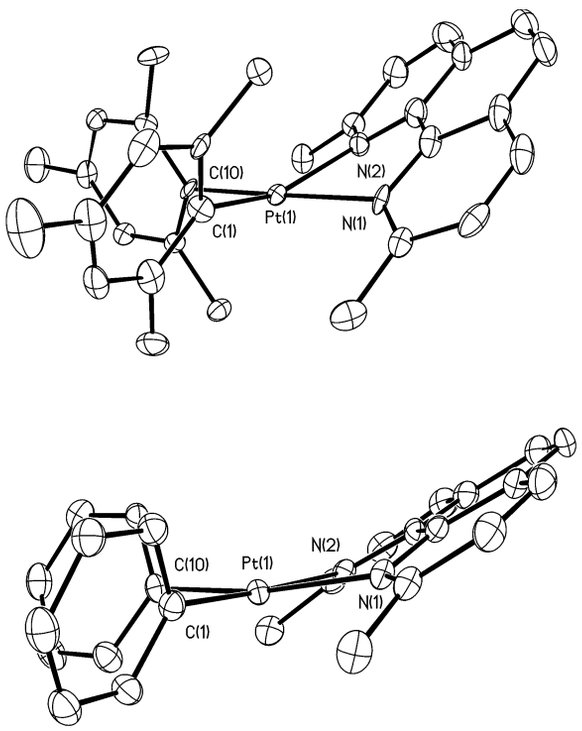

Fig. 2 Perspective views of the molecular structure of [(2,9-dmphen)-$PtMes_2$] (top) and [(2,9-dmphen)$PtPh_2$] (bottom).

co-ligands. Comparison with related diphenylplatinum complexes with other α-diimine ligands reveals similar values.[20] We therefore suppose that the angle is governed by electronic interaction of the phenyl ligand with the π-system of the diimine and that this quite constant value of about 70° provides optimum overlap. Support for this idea comes from recent quantum chemical calculations on such arylplatinum complexes.[20b] Comparison of the different dmphen complexes reveals the steric requirements of the co-ligands. The distortion effects increase in the series Ph < Cl < Mes < I, placing the mesityl group only slightly below the very big iodide ligands (Table 4).

Electrochemistry

The electrochemical properties of the platinum complexes were examined by cyclic voltammetry in THF solutions, Table 5 lists the corresponding data. All complexes exhibit a first reversible one-electron reduction wave and a second reduction wave that is at best only partly reversible. For the first reduction potentials of the dimesitylplatinum complexes we found a trend in decreasing values along the series phen > 5,6-dmphen > 2,9-dmphen > 4,7-dmphen > 3,8-dmphen > tmphen. This series of increased electron density donated by the methyl substituents fits nicely for the assumed target orbital to be mainly the $^2B_1$-LUMO (Scheme 1) of the phenanthroline system. Substitution on the 3-, 4-, 7-, or 8-position destabilises the $^2B_1$ level giving rise to more negative reduction potentials. However these results do not give any indication for a switch to the $^2A_2$ level to be the lowest orbital. Within the three 2,9-dmphen complexes the reduction potential decreases along the series $PtPh_2$ > $PtMes_2$ > $PtMe_2$. This parallels the decreasing electron density of the metal fragments. The dimesitylplatinum complexes all show reversible one-electron oxidation waves with half-wave potentials essentially the same for all compounds. The same behaviour was reported for other dimesitylplatinum complexes of α-diimine ligands, where the oxidation occurs at the platinum centre yielding the corresponding Pt(III) species.[12]

EPR spectroscopy on the radical anions

Electrochemical reduction of the parent complexes yielded persistent radical anion complexes of which the spectra obtained at ambient temperature in fluid solution did not show any hyperfine splitting with the exception of [(tmphen)PtMes]$^{\bullet -}$, Table 6. X-Band spectra taken from glassy frozen solutions at 110 K also showed insufficient resolution of the *g* components. We have, therefore, embarked on a multi-frequency EPR study, in conjunction with spectral simulation in order to define the spin-Hamiltonian parameters (*g*, *A*). Measurement of EPR spectra at more than one microwave frequency has many advantages over the usual single frequency studies (commonly X-band). For systems with small *g*-value anisotropy a high frequency measurement, *e.g.* Q-band (*ca.* 34 GHz) will enhance resolution of individual *g* components. However, a larger experimental linewidth is commonly observed at higher microwave frequencies due to the combined effects of *g*- and *A*-strain.[16] This can often result in the loss of resolution of hyperfine splitting. In some cases, a useful compromise is the application of the intermediate frequency, K-band (*ca.* 24 GHz). Similarly, if there is a reasonably large *g*-anisotropy but poorly resolved hyperfine splitting in the X-band spectrum, a low frequency measurement, *e.g.* S-band, *ca.* 4 GHz, may be warranted. The drawback here would be the diminished *g*-resolution and the inherently poorer sensitivity of lower frequencies. Accordingly, a multi-frequency approach is

Table 3 Bond angles (°) for [(2,9-dmphen)$PtPh_2$] and [(2,9-dmphen)$PtMes_2$] in comparison with [(phen)$PtMes_2$] (ref. 7)

	[(2,9-dmphen)$PtPh_2$]	[(2,9-dmphen)$PtMes_2$]	[(phen)$PtMes_2$]
C(1)–Pt(1)–C(10)	85.7(2)	88.4(4)	94.4(2)
C(1)–Pt(1)–N(1)	98.7(2)	94.7(4)	94.0(2)
C(10)–Pt(1)–N(1)	170.4(2)	176.8(3)	170.9(2)
C(1)–Pt(1)–N(2)	175.4(2)	159.2(4)	173.1(2)
C(10)–Pt(1)–N(2)	97.2(2)	99.9(3)	92.5(2)
N(1)–Pt(1)–N(2)	77.95(14)	77.0(3)	79.2(2)
Pt(1)–C(1)–C(2)	122.6(3)	127.6(8)	123.4(4)
Pt(1)–C(1)–C(6)	121.1(3)	116.4(7)	120.8(4)
Pt(1)–C(10)–C(11)	119.9(3)	122.3(7)	120.9(4)
Pt(1)–C(10)–C(15)	124.2(4)	122.0(7)	123.2(4)
Pt(1)–N(1)–C(19)	130.3(3)	129.7(7)	129.2(4)
Pt(1)–N(1)–C(30)	109.6(3)	110.9(6)	113.2(3)
C(19)–N(1)–C(30)	118.2(4)	118.1(8)	117.5(4)
Pt(1)–N(2)–C(28)	130.7(3)	131.8(7)	129.2(4)
Pt(1)–N(2)–C(29)	110.1(3)	107.7(6)	112.8(3)
C(28)–N(2)–C(29)	118.4(4)	117.7(9)	118.1(5)

Table 4 Structural parameters for complexes [(2,9-dmphen)PtX_2]

	X				
Dihedral angles (δ)	Mes	Ph	Cl	I	[(phen)$PtMes_2$]
N(1)–Pt(1)–N(2)/N(1)C(30)C(29)N(2)	28.1	23.3	27.5	29.7	3.8
C(1)–Pt(1)–C(10)/N(1)C(30)C(29)N(2)	42.8	31.3	38.8	44.0	6.4
C(1)–Pt(1)–C(10)/C(1)—C(6)	66.0	76.2	—	—	72.3
C(1)–Pt(1)–C(10)/C(10)—C(15)	70.7	73.6	—	—	69.4
N(1)C(19)—C(30) N(2)C(28)—C(29)[a]	12.3	7.6	16.6	15.3	1.4
deviation from best planes/Å					
[Pt(1)]/[N(1)N(2)C(1)C(10)	0.173	0.106	0.159	0.222[b]	0.036

[a] Dihedral angle between "pyridyl" rings; 1.3° in 2,9-dmphen·0.5H_2O. [b] Value from [(4,7-Ph_2-2,9-dmphen)PtI_2] (ref. 13c).

Table 5 Electrochemical data of platinum complexes[a]

Compound	E_{pa}(Ox2)[b]	$E_{1/2}$(Ox2)[c]	$E_{1/2}$(Red1)[c]	$E_{1/2}$(Red2)[c]
[(phen)$PtMes_2$]	0.97	0.45 (75)	−1.93 (61)	−2.60 (120)
[(5,6-dmphen)$PtMes_2$]	1.08	0.45 (74)	−2.10 (73)	−2.78 (111)
[(4,7-dmphen)$PtMes_2$]	n.o.[d]	0.43 (78)	−2.18 (66)	−2.78 (93)
[(3,8-dmphen)$PtMes_2$]	n.o.	0.44 (84)	−2.19 (81)	−2.80 (80)
[(2,9-dmphen)$PtMes_2$]	0.96	0.43 (81)	−2.17 (84)	−2.91 irr.[e]
[(2,9-dmphen)$PtPh_2$]	n.o.	1.02 irr.[b]	−2.12 (76)	−2.80 irr.[e]
[(2,9-dmphen)$PtMe_2$]	n.o.	1.01 irr.[b]	−2.24 (87)	−2.62 irr.[e]
[(tmphen)$PtMes_2$]	1.00	0.42 (79)	−2.28 (74)	−2.91 (111)

[a] From cyclic voltammetry in 0.1 M Bu_4NPF_6–THF solutions. Potentials in V *vs.* the ferrocene/ferrocenium couple, scan rate 100 mV s^{-1}. [b] Anodic peak potentials E_{pa} for irreversible oxidations. [c] Half-wave potentials $E_{1/2}$ for reversible or partly reversible waves, peak potential differences $\Delta E_{pp} = E_{pa} - E_{pc}$ in mV (in parentheses). [d] n.o. = not observed. [e] Cathodic peak potentials E_{pc} for irreversible reductions.

Table 6 EPR data of anion radical complexes $[(NN)PtR_2]^{-\bullet}$[a]

Radical[b]	g_1	g_2	g_3	$g_{iso,calc.}$[c]	Δg[d]	a_1	a_2	a_3
[(tmphen)$PtMes_2$]$^{\bullet-}$(DMF)	2.023	2.002	1.905	1.977	1180	[f]	[f]	[f]
[(tmphen)$PtMes_2$]$^{\bullet-}$(THF)	2.010	2.004	1.935	1.983	750	[f]	[f]	[f]
[(5,6-dmphen)$PtMes_2$]$^{\bullet-}$	2.028	2.003	1.914	1.982	1140	30	34	(15)[g]
[(4,7-dmphen)$PtMes_2$]$^{\bullet-}$	2.023	2.002	1.904	1.977	1190	30	30	(15)[g]
[(3,8-dmphen)$PtMes_2$]$^{\bullet-}$	2.027	2.002	1.901	1.977	1260	30	34	(15)[g]
[(2,9-dmphen)$PtMes_2$]$^{\bullet-}$	2.018	2.012	1.921	1.984	970	30	30	(15)[g]
[(2,9-dmphen)$PtPh_2$]$^{\bullet-}$[e]	2.026	2.013	1.916	1.985	1100	27	30	—
[(2,9-dmphen)$PtMe_2$]$^{\bullet-}$[e]	2.038	2.025	1.905	1.990	1330	26	33	—
[(phen)$PtMes_2$]$^{\bullet-}$	2.028	2.002	1.906	1.979	1220	29	33	(15)[g]
[(bpy)$PtMes_2$]$^{\bullet-}$	2.031	2.005	1.934	1.990	970	53	87	(15)[g]

[a] All values are from spectral simulations of the S-, X- and Q-band spectra in glassy frozen solutions at 110 K, coupling constants $a(^{195}Pt)$ in Gauss. [b] Paramagnetic species generated by electrolysis in THF or DMF solutions containing 0.1 M Bu_4NPF_6. [c] $g_{iso,calc} = [(g_1^2 + g_2^2 + g_3^2)/3]^{1/2}$. [d] $\Delta g = g_1 - g_3 \times 10^4$. [e] From X-band spectra only. [f] Not determined (not resolved). [g] Assumed value used for spectral simulation.

most advantageous. The experimental parameters are best determined by computer simulation of spectra at different frequencies, using a consistent set of parameters (g, A).

The spectra of [(3,8-dmphen)$PtMes_2$]$^{\bullet-}$ as shown in Fig. 3 are typical for the dimesityl platinum complexes with phen, 5,6-dmphen, 4,7-dmphen, 3,8-dmphen (in DMF or THF

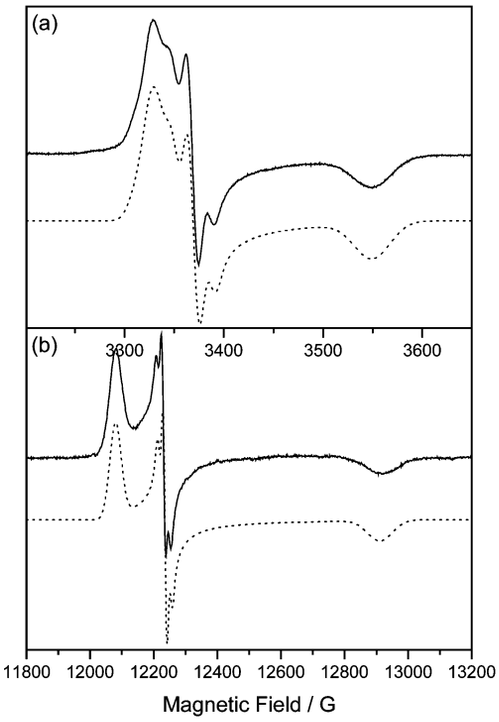

Fig. 3 EPR spectra of $[(3,8\text{-dmphen})PtMes_2]^{\bullet -}$ at 110 K in glassy frozen DMF solution at X-band (a), and Q-band frequency (b) with simulations shown below.

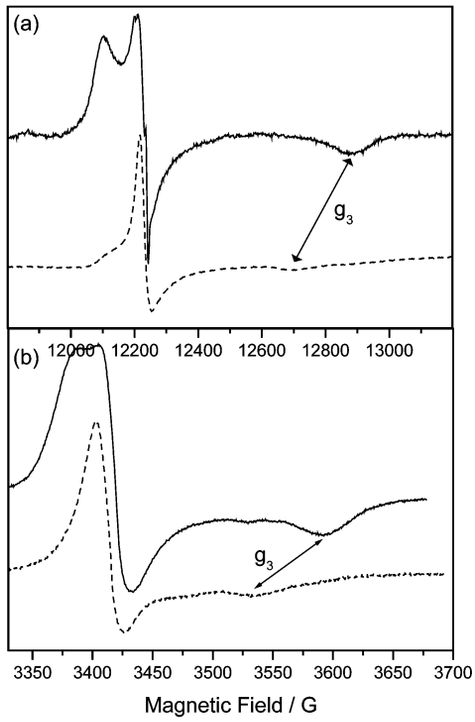

Fig. 5 EPR spectra of $[(tmphen)PtMes_2]^{\bullet -}$ at 110 K in glassy frozen solutions of DMF (solid lines) or THF (dotted lines) at Q-band frequency (a) and X-band frequency (b).

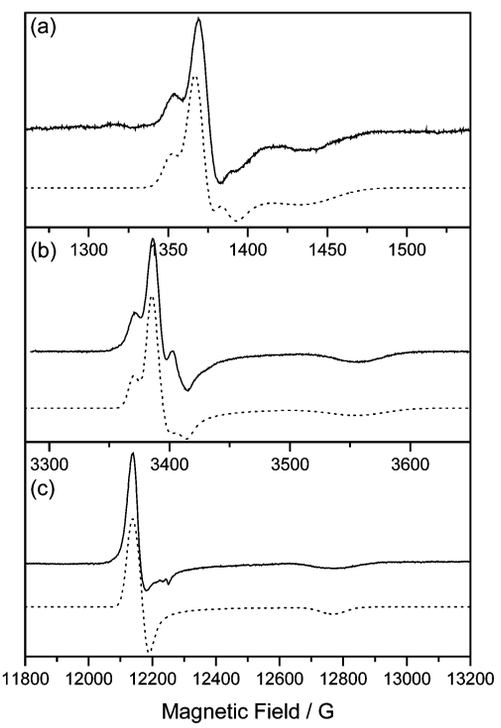

Fig. 4 EPR spectra of $[(2,9\text{-dmphen})PtMes_2]^{\bullet -}$ at 110 K in glassy frozen DMF solution at S-band (a), X-band (b), and Q-band frequency (c) with simulations shown below.

solution), and tmphen (in THF solution). The spectra of $[(2,9\text{-dmphen})PtMes_2]^{\bullet -}$ (Fig. 4) and $[(tmphen)PtMes_2]^{\bullet -}$ (in DMF, Fig. 5) are markedly different.

The isotropic *g*-values (g_{iso}) are rather similar for all complexes under investigation which suggests that the frontier orbital situation is comparable for all complexes, best described by metal orbitals forming the highest occupied molecular orbitals (from electrochemical evidence) whereas the singly occupied molecular orbital (SOMO) is predominantly located on the lowest π* orbital of the diimine ligand with further π* orbitals in energetic proximity ($g_{iso} < 2$).[21,22] The isotropic coupling constant a_{Pt} (a_1 and a_2, coupling to the ^{195}Pt isotope, $I = 1/2$, 33.8% natural abundance) were also rather invariant within the series of phenanthroline complexes. The bpy complex however showed much higher coupling constants. Generally it is assumed, that the metal coupling constants are a good measure to estimate the contribution of platinum orbitals to the unpaired electron.[21] Therefore we have to conclude that the platinum contribution is higher for bpy than for the phenanthroline complex. Unfortunately, the incomplete data set (a_3 is never observed) precludes unequivocal conclusions based on semi-empirical calculations. As recently established the *g*-anisotropy is also meaningful in considering the metal contribution in such organoplatinum radicals.[17] High Δg goes along with high metal contribution, therefore, we conclude from the present data that the platinum contributions vary slightly within the series of the complexes under investigation with unusually low values for $[(tmphen)PtMes_2]^{\bullet -}$ (in THF), $[(2,9\text{-dmphen})PtMes_2]^{\bullet -}$ and $[(bpy)PtMes_2]^{\bullet -}$. The finding for the latter complex appears contradictory to the findings of the coupling constants. We propose the following qualitative explanation for this: the phenanthroline ligands provide a rigid framework that enables effective electron delocalization within the platinum + ligand core. Upon reduction the odd electron is delocalized in this core. In contrast to this the bipyridine ligand in such complexes is predicted to undergo a tilt of the two pyridine units upon reduction leading to reduced delocalization of the unpaired electron. Thus higher metal contribution is expected for the phenanthroline system. The coupling constants are probably governed by the electron density on the binding nitrogen centres which is markedly higher for bpy as inferred from simple HMO considerations. The assumption that distortion of the ligand + platinum system leads to decreased *g*-anisotropy (= decreased metal contribution) is supported by the finding that the highly distorted system $[(2,9\text{-dmphen})PtMes_2]^{\bullet -}$ exhibits an unusually small Δg whereas the coupling constants are in the range of other dmphen complexes. The corresponding diphenyl and the dimethyl complex display the

Table 7 Long-wavelength absorption maxima λ_{max} (nm) of neutral platinum complexes

Compound	Solvent	λ_1 (ε)[a]	λ_2 (ε)[a]
[(5,6-dmphen)$PtMes_2$]	toluene	396sh, 416, 453, 495	549sh
	THF	333, 402, 445, 471	530sh
	CH_3CN	347sh, 388, 429sh, 458sh	—
[(4,7-dmphen)$PtMes_2$]	toluene	387sh, 406, 448, 481	530sh
	THF	367sh, 394, 439, 463	517sh
	CH_3CN	351sh, 384, 419sh, 445sh	—
[(3,8-dmphen)$PtMes_2$]	toluene	345sh, 399, 448, 469	552sh
	THF	340sh, 390(1.9), 438(1.7), 458sh	520sh(0.3)
	CH_3CN	360sh, 381sh, 419, 441	—
[(2,9-dmphen)$PtMes_2$]	toluene	346sh, 418, 439sh, 497	—
	THF	388sh, 401(2.5), 470(2.1)	—
	CH_3CN	344sh, 387, 408sh, 449	—
[(2,9-dmphen)$PtPh_2$]	toluene	346sh, 384, 438, 461	—
	THF	322sh, 372(3.1), 426(2.5), 438(2.6)	—
	CH_3CN	353sh, 412	—
[(phen)$PtMes_2$]	toluene	387sh, 420, 447, 500	530sh
[(tmphen)$PtMes_2$]	toluene	367sh, 398, 443, 468	523sh

[a] Molar extinction coefficients ε (10^3 dm^3 mol^{-1} cm^{-1}), for assignments see text, principal maxima are underlined.

normal behaviour. The most astonishing results were achieved for [(tmphen)$PtMes_2$]$^{\bullet -}$. We found at 110 K in glassy frozen THF solution a rhombic spectrum with g_1 = 2.010, g_2 0 2.004 and g_3 = 1.935. The g_3 component was not found in the previously reported experiments[7] and the g anisotropy (Δg) given therein of 141 must be corrected to 750. Moreover in glassy frozen DMF solution we found rhombic spectra with different g values and a markedly higher g anisotropy, comparable to the other examples. For the other complex no such solvent dependence was found. This extraordinary behaviour might be explained by an anticipated alternation in the character of the SOMO ($^2B_1$ *vs.* $^2A_2$). If the $^2A_2$ level is favoured this should result in a smaller contribution of Pt metal orbitals (small Δg).[7] This seems to be the case in THF solution. Occupancy of the $^2B_1$ level results in a higher contribution from platinum orbitals through increased coefficients on the nitrogen donor centres. This seems to be the case in the very polar solvent DMF. Although these results have been reproduced several times at present we do not wish to draw final conclusions. Further experiments mainly focussing on ENDOR spectroscopy in various solvents should be executed. The hyperfine coupling patterns to the ^1H should be very different for the two different ground states.

UV/Vis/NIR absorptions (spectroelectrochemistry)

The orange to red coloured parent complexes exhibit several long-wavelength absorption maxima in fluid solution between 400 and 500 nm (Table 7). They are of medium intensity (ε = 1700–3100 dm^3 mol^{-1} cm^{-1}) and exhibit negative solvatochromic behaviour which allows us to assign them to metal-to-ligand charge transfer (^{1}MLCT) transitions.[12,22,23] Whether the multiple maxima are due to several transitions or vibrational fine structuring is the subject of current investigations. The energy of the lowest absorptions maximum increases in the series phen ≤ 2,9-dmphen ≤ 5,6-dmphen < 4,7-dmphen < 3,8-dmphen ≤ tmphen which parallels the reduction potentials. In less polar solvents further weak absorptions can be observed at even lower energy. We assign these to the corresponding triplet charge transfer excitations (^{3}MLCT).[12,23,24]

The one-electron reduced complexes all show several, in some cases markedly structured, absorption bands over the entire spectral region (200–2400 nm). The low energy transitions (Table 8) are assigned to transitions from the singly occupied molecular orbital (SOMO) to higher lying π* orbitals of the phenanthroline ligand. These transitions are symmetry forbidden and are hardly observed for the free ligands. In the present complexes the coordination to the heavy element platinum with its high spin orbit coupling constant and the geometric distortion on coordination leads to an increase in intensity. Consequently we found the highest intensities in our series for the complex [2,9-dmphen$PtMes_2$]$^{\bullet -}$. Within the timescale of the spectroelectrochemical experiments the first reductions are fully reversible. Upon further reduction all transitions shift to higher energies, which is expected for the double occupation of the π* orbital at the ligand. However, the dianionic species are of much lesser stability than the monoanions, therefore their spectral characterization is doubtful in some cases where the second reduction waves turned out to be not fully reversible.

Experimental

Spectroscopic measurements

^{1}H-NMR spectra were recorded on a Bruker AC 250 spectrometer. Cyclic voltammetry was carried out using a three-electrode configuration (glassy carbon working electrode, platinum counter electrode, Ag/AgCl reference) and a PAR 273 potentiostat and function generator with PAR M270/250 software. As internal standard the ferrocene/ferrocenium couple ($FeCp_2^{+/0}$) was employed. UV/Vis/NIR absorption spectra were recorded on a Bruins Instruments Omega 10 spectrophotometer. UV/Vis/NIR spectroelectrochemical measurements were performed using an optical transparent thin-layer electrode (OTTLE) cell.[25] *In situ* EPR spectroelectrochemical studies were performed using a platinum two-electrode cell at K and Q-band where the size of the EPR tubes prevented use of a 3-electrode assembly. Although this does not allow accurate potential control, the EPR spectra obtained were consistent with those obtained at X-band with a proper 3-electrode cell, which gives an important test of the integrity of the paramagnetic species being generated. EPR spectra of glassy frozen solutions at 110 K were recorded on a Bruker ESP300E spectrometer using Bruker ER4118SPT–N1 (S), ER4102ST (X), ER6706KT (K) and an ER5106QT (Q-band) resonators. Magnetic fields and microwave frequencies were measured with an ER035M NMR gaussmeter and an EIP model 588C microwave pulse counter, respectively. EPR spectra in fluid solution at ambient temperatures were recorded at X band on a Bruker System ESP 300 equipped with a Bruker ER035M gaussmeter and a HP 5350B microwave counter. Simulations of EPR spectra were performed using in-house software.[16]

Materials and procedures

Synthetic procedures for the ligand 3,8-dmphen [6] and for the complexes [(dmphen)$PtMes_2$][12] have been described. The latter

Table 8 Long-wavelength absorption maxima of anion radical and dianionic complexes[a]

Compound	λ_{max} (ε)[b]		
[(5,6-dmphen)$PtMes_2$]$^{\bullet -}$	486, 543, 578	639, 707, 786, 889	1407, 1824, 2140
[(4,7-dmphen)$PtMes_2$]$^{\bullet -}$	517, 560, 606	657sh, 737, 826, 939, 992	1365, 1811, 2120
[(3,8-dmphen)$PtMes_2$]$^{\bullet -}$	590, 630 (1.7)	714, 812 (0.3), 923	1360, 1712 (0.1), 2115
[(2,9-dmphen)$PtMes_2$]$^{\bullet -}$	592, 637 (2.7)	707, 796 (0.7), 895	1343, 1660 (0.3), 2194
[(2,9-dmphen)$PtPh_2$]$^{\bullet -}$	601sh, 641 (2.0)	701sh, 794 (0.2), 898	1213, 1614 (0.05), 2161
[(tmphen)$PtMes_2$]$^{\bullet -}$	564, 610 (3.7)	741, 845 (1.4), 955	1480, 1783 (0.1), 1975
[(phen)$PtMes_2$]$^{\bullet -}$	569, 616(1.9)	655sh, 720, 808 (0.4), 910	1234, 1611 (0.2), 1980
[(5,6-dmphen)$PtMes_2$]$^{2-}$	389sh	650	791
[(4,7-dmphen)$PtMes_2$]$^{2-}$	422	616	740sh, 780
[(3,8-dmphen)$PtMes_2$]$^{2-}$	407sh	626, 666sh	794
[(2,9-dmphen)$PtMes_2$]$^{2-}$	425	584	862

[a] Generated by cathodic reduction of neutral compounds in 0.1 M Bu_4NPF_6–THF solutions (OTTLE spectroelectrochemistry). [b] Absorption maxima in nm, molar extinction coefficients ε (in 10^3 dm^3 mol^{-1} cm^{-1}) in parentheses; principal bands underlined.

were obtained in 80–90% yield as orange microcrystals and analyzed correctly (see Table S1, ESI†). The compounds [(2,9-dmphen)$PtPh_2$] and [(2,9-dmphen)$PtMe_2$] were prepared from [(COD)$PtPh_2$],[26] or [$(Me_2Pt(\mu\text{-}SMe_2)_2PtMe_2$],[27] respectively, according to established procedures.[28,29]

[(2,9-dmphen)$PtPh_2$]

Yellow powder, 86% yield. Anal. Calc. for $C_{26}H_{22}N_2Pt$: C, 56.01; H, 3.98; N, 5.02. Found: C, 55.89; H, 3.51; N, 4.95%. ^{1}H-NMR in acetone-d^6 δ: 8.64 (d, 2H, ^3J(H4-H3) = 8.35 Hz, H4,7), 8.06 (s, 2H, H5,6), 7.70 (d, 2H, H3,8), 7.36 (d, 4H, ^3JPt-*o*H = 74.45 Hz, ^3J*o*H-*m*H = 8.03, *o*Ph), 6.73 (t, 4H, ^3J*m*H-*p*H = 7.02, *m*Ph), 6.30 (t, 2H, *p*Ph), 2.15 (s, 2H, $^{2,9}CH_3$).

[(2-9-dmphen)$PtMe_2$]

Orange microcrystals, 81% yield. Anal. Calc. for $C_{18}H_{18}N_2Pt$: C, 47.26; H, 3.97; N, 6.12. Found: C, 44.58; H, 3.51; N, 5.87%. ^{1}H-NMR in CD_2Cl_2 δ: 8.35 (d, 2H, ^2J(H3-H4) = 8.26 Hz, H4,7), 7.98 (s, 2H, H5,6), 7.80 (d, 2H, H3,8), 2.12 (s, 6H, $^{2,9}CH_3$), 0.66 (s, 6H, ^2J(Pt-CH_3) = 82.80 Hz).

Crystal structure analysis

For both compounds the data collection was performed on a Siemens P4 diffractometer with MoK_α radiation (λ = 0.71073 Å), using an empirical absorption correction (ψ-scan). The structures were solved by direct methods using the SHELXTL-PLUS package,[30] refinement was carried out with SHELXL97 employing full-matrix least-squares methods on F^2.[31] All non-hydrogen atoms were treated anisotropically, hydrogen atoms were included using the riding model. The main crystal details are summarised in Table 1.

CCDC reference numbers 179188 and 179189.

See http://www.rsc.org/suppdata/dt/b2/b201419j/ for crystallographic data in CIF or other electronic format.

Summary

A series of dimesitylplatinum complexes of isomeric, symmetrically substituted dimethylphenanthrolines were synthesised and studied electrochemically and spectroscopically. The molecular structure of the 2,9-substituted phenanthroline complex reveals steric interactions of the methyl substituents on the phen ligand with the mesityl substituents on the platinum resulting in large distortions from square planar. Comparison with the analogous diphenylplatinum complex explicitly reveals the interaction of the methyl substituents on both the phenanthroline ligand and mesityl substituent. The new complexes undergo reversible one-electron reduction and the resulting radical anions were examined by optical spectroscopy and EPR. Multi-frequency EPR experiments were performed to maximise resolution of the Hamilton parameters g and A. However, the lack of resolution of the platinum HF coupling in fluid solution and in the g_3 component in frozen solution (as also found in studies of similar species) precludes quantitative determination of the contribution of platinum orbitals to the SOMO. Instead we can use the g-anisotropy Δg (= $g_1 - g_3$) as a good qualitative tool. Within the series of phenanthroline complexes the variation in Δg is rather small with two marked exceptions. The severely distorted 2,9-dmphen complex exhibits an unusually small Δg which supports the explanation above. Furthermore, the trend in Δg for the 2,9-dmphen complexes is $PtMes_2 < PtPh_2 < PtMe_2$ (Table 6) which supports the idea that a decrease in planarity leads to an decrease in Δg. The tmphen complex as measured in a THF glass also reveals a very diminished Δg whereas in DMF the behaviour is as found for the others. We tentatively assign this to a solvent induced alternation in the character of the SOMO ($^2B_1$ *vs.* $^2A_2$). In THF the $^2A_2$ level is operating, resulting in smaller contribution of Pt metal orbitals (small Δg) whereas in the very polar solvent DMF a switch to occupancy of the $^2B_1$ level can be observed resulting in higher contribution from platinum orbitals through increased coefficients on the nitrogen donor centres.

Acknowledgements

We thank Dr. Peter Belser, University of Fribourg (Switzerland), for a sample of 3,8-dimethyl-1,10-phenanthroline and Dr. Mark Niemeyer, University of Stuttgart, for assistance with the crystal structure determination. Dr. Frank Mabbs is acknowledged for helpful discussions and facilities at the EPSRC c.w. EPR Service Centre, in the Department of Chemistry, The University of Manchester.

References

1 (*a*) M. Hissler, J. E. McGarrah, W. B. Connick, D. K. Geiger, S. D. Cummings and R. Eisenberg, *Coord. Chem. Rev.*, 2000, **208**, 115; (*b*) K. Base, M. T. Tierney, A. Fort, J. Muller and M. W. Grinstaff, *Inorg. Chem.*, 1999, **38**, 287.

2 (*a*) V. H. Houlding and V. M. Miskowski, *Coord. Chem. Rev.*, 1991, **111**, 145; (*b*) V. M. Miskowski and V. H. Houlding, *Inorg. Chem.*, 1991, **30**, 4446; (*c*) V. M. Miskowski and V. H. Houlding, *Inorg. Chem.*, 1989, **28**, 1529; (*d*) R. Schwarz, M. Lindner and G. Gliemann, *Ber. Bunsen-Ges. Phys. Chem.*, 1987, **91**, 1233.

3 (*a*) K.-H. Wong, M. C.-W. Chan and C.-M. Che, *Chem. Eur. J.*, 1999, **5**, 2845; (*b*) C.-W. Chan, L.-K. Cheng and C.-M. Che, *Coord. Chem. Rev.*, 1994, **132**, 87.

4 (*a*) V. V. Rostovtsev, J. A. Labinger and J. E. Bercaw, *Organometallics*, 1998, **17**, 4530; (*b*) R. A. Periana, D. J. Taube, S. Gamble, H. Taube, T. Satoh and H. Fujii, *Science*, 1998, **280**, 560.

5 (*a*) S. D. Ittel, L. K. Johnson and M. Brookhart, *Chem. Rev.*, 2000, **100**, 1169; (*b*) S. Mecking, *Angew. Chem.*, 2001, **113**, 550; (*c*) A. M. LaPointe and M. Brookhart, *Organometallics*, 1998, **17**, 1530;

(*d*) A. M. LaPointe, F. C. Rix and M. Brookhart, *J. Am. Chem. Soc.*, 1997, **119**, 906.
6 P. Belser, S. Bernhard and U. Guerig, *Tetrahedron*, 1996, **52**, 2937.
7 A. Klein, W. Kaim, E. Waldhör and H.-D. Hausen, *J. Chem. Soc., Perkin Trans.*, 1995, 2121.
8 T. Koizumi, Y. Yokohame, K. Morihashi, M. Nakayama and O. Kikuchi, *Bull. Chem. Soc. Jpn.*, 1992, **65**, 2839.
9 S. Ernst, C. Vogler, A. Klein, W. Kaim and S. Zalis, *Inorg. Chem.*, 1996, **35**, 1295.
10 W. Kaim, *J. Am. Chem. Soc.*, 1982, **104**, 3833.
11 A. Klein, H.-D. Hausen and W. Kaim, *J. Organomet. Chem.*, 1992, **440**, 207.
12 A. Klein and W. Kaim, *Organometallics*, 1995, **14**, 1176.
13 (*a*) R. J. H. Clark, F. P. Fanizzi, G. Natile, C. Pacifico, C. G. van Rooyen and D. A. Tocher, *Inorg. Chim. Acta*, 1995, **235**, 205; (*b*) F. P. Fanizzi, F. P. Intini, L. Maresca, G. Natile, M. Lanfrachi and A. Tiripicchio, *J. Chem. Soc., Dalton Trans.*, 1991, 1007; (*c*) F. P. Fanizzi, G. Natile, M. Lanfranchi, A. Tiripicchio, F. Laschi and P. Zanello, *Inorg. Chem.*, 1996, **35**, 3173.
14 (*a*) V. G. Albano, M. L. Ferrara, M. Monari, A. Panunzi and F. Ruffo, *Inorg. Chim. Acta*, 1999, **285**, 70; (*b*) V. G. Albano, M. Monari, I. Orabona, F. Ruffo and A. Vitagliano, *Inorg. Chim. Acta*, 1997, **265**, 35; (*c*) F. Giordano, F. Ruffo, A. Saporito and A. Panunzi, *Inorg. Chim. Acta*, 1997, **264**, 231; (*d*) F. P. Fanizzi, L. Maresca, G. Natile, M. Lanfranchi, A. Tiripicchio and G. Pacchioni, *J. Chem. Soc., Chem. Commun.*, 1992, 333; (*e*) R. Romeo, L. Monsù Scolaro, N. Nastasi and G. Arena, *Inorg. Chem.*, 1996, **35**, 5087.
15 O. Clement, D. H. Macartney and E. Buncel, *Inorg. Chim. Acta*, 1997, **264**, 117.
16 F. E. Mabbs and D. Collison, *Electron Paramagnetic Resonance of d Transition Metal Compounds*, Elsevier, Amsterdam, 1992.
17 A. Klein, E. J. L. McInnes, T. Scheiring and S. Zalis, *J. Chem. Soc., Faraday Trans.*, 1998, 2979.
18 W. B. Connick, R. E. Marsh, W. P. Schaefer and H. B. Gray, *Inorg. Chem.*, 1997, **36**, 913.
19 H.-A. Brune, R. Klotzbücher, K. Berhalter and T. Debaerdemaeker, *J. Organomet. Chem.*, 1989, **369**, 321 and references therein.
20 (*a*) Y.-Y. Ng, C.-M. Che and S.-M. Peng, *New J. Chem.*, 1996, **20**, 781; (*b*) A. Klein, J. van Slageren and S. Zális, crystal structure of [(tap)$PtPh_2$], manuscript in preparation.
21 (*a*) E. J. L. McInnes, R. D. Farley, S. A. Macgregor, K. J. Taylor, L. J. Yellowlees and C. C. Rowlands, *J. Chem. Soc., Faraday Trans.*, 1998, 2985; (*b*) D. Collison, F. E. Mabbs, E. J. L. McInnes, K. J. Taylor, A. J. Welsh and L. Y. Yellowlees, *J. Chem. Soc., Dalton Trans.*, 1996, 329; (*c*) E. J. L. McInnes, R. D. Farley, C. C. Rowlands, A. J. Welch, L. Rovatti and L. J. Yellowlees, *J. Chem. Soc., Dalton Trans.*, 1999, 4203; (*d*) E. J. L. McInnes, R. D. Farley, S. A. Macgregor, K. J. Taylor, L. J. Yellowlees and C. C. Rowlands, *J. Chem. Soc., Faraday Trans.*, 1998, **94**, 2985.
22 P. S. Braterman, J.-I. Song, C. Vogler and W. Kaim, *Inorg. Chem.*, 1992, **31**, 222.
23 R. H. Hill and R. J. Puddephatt, *J. Am. Chem. Soc.*, 1985, **107**, 1218.
24 G. A. Crosby and K. R. Kendrick, *Coord. Chem. Rev.*, 1998, **171**, 407 and references therein.
25 M. Krejcik, M. Danek and F. Hartl, *J. Electroanal. Chem.*, 1991, **317**, 179.
26 C. R. Kistner, J. H. Hutchinson, J. R. Doyle and J. C. Storlie, *Inorg. Chem.*, 1963, **2**, 1255.
27 J. D. Scott and R. J. Puddephatt, *Organometallics*, 1983, **2**, 1643.
28 C. Vogler, B. Schwederski, A. Klein and W. Kaim, *J. Organomet. Chem.*, 1992, **436**, 367.
29 P. K. Monaghan and R. J. Puddephatt, *Organometallics*, 1984, **3**, 444.
30 G. M. Sheldrick, SHELXTL-Plus, An Integrated System for Solving, Refining and Displaying Crystal Structures from Diffraction Data, Siemens Analytical X-Ray Instruments Inc., Madison, WI, 1989.
31 G. M. Sheldrick, SHELXL-97, Program for Crystal Structure Determination, Universität Göttingen, Germany, 1997.